

METHODS FOR THE SURFACE REFLECTANCE RETRIEVAL FROM CHRIS/PROBA DATA OVER LAND AND INLAND WATERS

Luis Guanter, Luis Alonso, and Jose Moreno

University of Valencia - Faculty of Physics, Dr. Moliner 50, 46100, Burjassot (Valencia), Spain.
EMAIL: luis.guanter@uv.es

ABSTRACT

The Compact High Resolution Imaging Spectrometer (CHRIS) on board the Project for On-Board Autonomy (PROBA) platform system provides the first high spatial resolution hyperspectral/multiangular remote sensing data from a satellite system, what represents a new source of information for Earth Observation purposes. When dealing with the retrieval of surface reflectance from such kind of hyperspectral data, a radiative transfer approach is commonly preferred. However, since CHRIS 2003 and 2004 data present reported calibration problems in several bands, especially in the near-infrared region, a standard atmospheric correction based on radiative transfer models should not be performed. A dedicated atmospheric correction algorithm for CHRIS/PROBA data over land is presented in this work. It consists in the combination of radiative transfer and empirical line approaches to atmospheric correction, in order to retrieve surface reflectance images free from both the atmospheric distortion and artifacts due to mis-calibration. The atmospheric optical parameters and the updated set of calibration coefficients are obtained jointly in an autonomous process, without the need for any ancillary data. Results from the application of the algorithm to CHRIS/PROBA data from the two ESA SPECTRA BARRAX Campaign (SPARC) held at the Barrax study site (La Mancha, Spain) in 2003 and 2004 are presented in this work, focusing on the validation of the final surface reflectance using in-situ measurements acquired simultaneously to PROBA overpasses. Besides, the first version of an atmospheric correction module for inland waters, which is currently under development, is also presented, as well as the first results obtained from its application to data from the Rosarito reservoir. The potential of CHRIS/PROBA data for Earth observation purposes is shown.

Key words: CHRIS/PROBA, Atmospheric correction, Surface reflectance, Radiative transfer, Empirical line, Calibration coefficients, SPARC campaign, Inland waters.

1. INTRODUCTION

The CHRIS/PROBA system [1], provides high spatial resolution hyperspectral/multiangular data, what constitutes a new generation of remote sensing information to be processed and exploited. On one hand, the PROBA platform provides pointing in both across-track and

along-track directions. In this way, the CHRIS/PROBA system has multiangular capabilities, acquiring up to 5 consecutive images from 5 different view zenith angles (VZA). Each imaged target has an associated “fly-by” position, that is the position on the ground track when the platform zenith angle, as seen from the target, is a minimum. The platform acquires the images at times when the zenith angle of the platform with respect to the fly-by position is equal to a set of Fly-by Zenith Angles (FZA): 0° , $\pm 36^\circ$ or $\pm 55^\circ$. Negative FZAs to acquisition geometries when the satellite has already flown over the target position.

On the other hand, CHRIS measures over the visible/near-infrared (NIR) bands from 400 nm to 1050 nm, with a minimum spectral sampling interval ranging between 1.25 (@400 nm) and 11 nm (@1000 nm). It can operate in different modes, compromising the number of spectral bands and the spatial resolution because of storage reasons. The data we are presenting in this work were acquired using operation Mode-1, with 62 spectral bands at a spatial resolution of 34 m. CHRIS/PROBA images have an approximate swath of 15 km.

In those visible and NIR wavelengths, the atmospheric influence is strong enough to modify the reflected electromagnetic signal. The main atmospheric species affecting the electromagnetic radiation in the visible and NIR spectral regions are ozone, aerosols, and water vapor. Those cause the loss or the corruption of part of the carried information about the observed target. Thus, any set of CHRIS/PROBA data needs for a previous removal of the atmospheric effects in the initial processing steps, to assure a maximal accuracy and reliability in the results inferred by the latter exploitation of the data. This is the fundamental basis of the atmospheric correction in optical remote sensing: the elimination of the atmospheric effects from the useful signal reflected by the observation target in the observer’s line of sight. A traditional statement of the problem can be found, for instance, in [2] or [3].

When dealing with accurately calibrated hyperspectral instruments, such as the Airborne Visible/InfraRed Imaging Spectrometer (AVIRIS) [4] or the HyMap sensor [5], a radiative transfer approach is usually preferred to achieve the best results in atmospheric correction [6, 7, 8]. In those methods, radiative transfer codes are used to calculate the atmosphere’s optical parameters, in order to remove the atmospheric contribution to the measured at-sensor radiances.

One of the most challenging issues in the radiative trans-

fer approach is the estimation of the concentrations of the main atmospheric species, which must be supplied to the radiative transfer code. The ozone concentration is quite well-known, due to its low spatial and temporal variability. An approximated value of ozone concentration for a given location can be obtained from several public databases [9, 10]. However, the situation is very different for aerosols and water vapor, whose concentrations are highly variable.

Therefore, in order to perform an accurate atmospheric correction, an estimate of aerosol and water vapor contents simultaneous to image acquisition is required. The common procedure for hyperspectral data uses associated algorithms for the retrieval of water vapor column content in a pixel by pixel basis [11, 12, 13]. In the case of aerosols, default climatology values are usually assumed for the aerosol optical thickness, although some methods for the retrieval from high spatial resolution hyperspectral data have been presented [14, 15]. All of these methods lie on sophisticated physical models, for which the reliability of the sensor's spectral calibration is fully required [16].

When such accuracy in the instrument's spectral calibration is not assure, alternative methods should be used to retrieve surface reflectance with a minimum error. A widely used approach in those conditions is the empirical line method [17, 18]. In its most general implementation, the empirical line method is based on the calculation of calibration coefficients from linear correlations between the radiances registered by the sensor for some reference pixels with surface reflectance spectra measured in-situ in the same points. The spectral uniformity of the target, its low temporal evolution and the availability of one or more bright pixels are assumed. In this way, not only the atmospheric distortion is removed, but also the artifacts due to spectral calibration problems. Therefore, this approach is likely to produce better results in the atmospheric correction of those instruments where calibration deficiencies are expected. Two main shortcomings can be highlighted: one is the dependency on simultaneous ground measurements, which are seldom available in usual processing chains. The other, the fact that the angular dependencies in the target are hardly taken into account, since most of the in-situ measurements are acquired from a nadir view. Those causes make standard empirical line methods can not be applied to series of multiangular CHRIS/PROBA imagery. Instead, the radiative transfer approach would be preferred.

However, since the CHRIS/PROBA system was designed as a technology demonstrator, limited resources were devoted to the construction of a high-profile sensor. For this reason, CHRIS presents some mis-calibration trends all over the covered spectral region [19], being the underestimation of the signal in the NIR wavelengths the most important one. Even though updated sets of calibration coefficients are planned for 2005 CHRIS/PROBA data releases [20], the spectral calibration of 2003 and 2004 data does not allow using complex radiative transfer algorithms for the retrieval of atmospheric constituents (especially water vapor) and surface reflectance. In order to illustrate this fact, sample surface reflectance spectra which would be obtained by a common radiative

transfer-based algorithm are plotted in Fig. 1 (thin line). The thick one corresponds to the results obtained by the method presented in this paper, where the calibration issue is addressed. One can notice the large mis-calibration of CHRIS data in the NIR region, which leads to the loss of the typical "plateau" shape expected for vegetation targets in those wavelengths, and the improvements achieved by means of the update of the calibration coefficients.

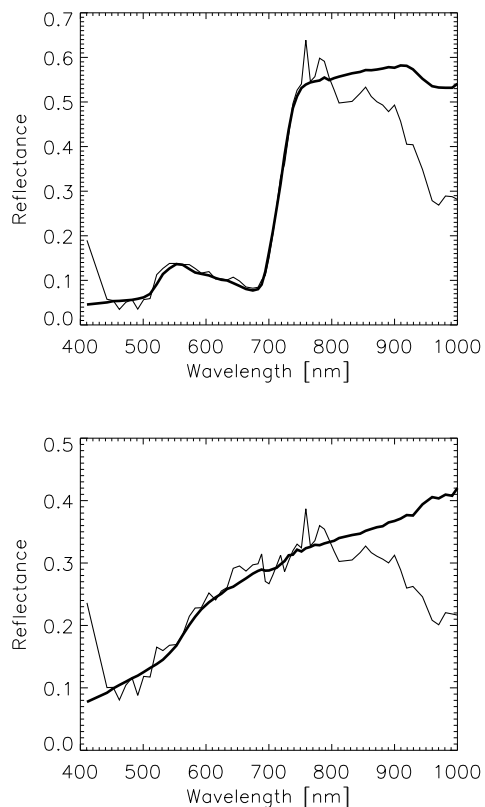


Figure 1. Comparison between sample surface reflectance spectra obtained from a common atmospheric correction method (thin line), based on a radiative transfer approach, and the methodology presented in this paper (thick line).

In this framework, a dedicated atmospheric correction algorithm for CHRIS/PROBA data over land has been developed. The idea is combining both the radiative transfer and the empirical line approaches, in order to derive the appropriate atmospheric parameters and a set of correction factors for CHRIS's gain coefficients altogether. One of the strongest points of the method is that it works in a fully automatic manner, without the need for any ground-based atmospheric or surface reflectance ancillary information. The fundamental basis lies on a multiparameter inversion of the Top-Of-Atmosphere (TOA) radiances from 5 reference pixels with a high spectral contrast, giving as a result the estimations of aerosol optical thickness (AOT) and water vapor content, as well as the calibration coefficients. All of these variables are used to derive the surface reflectance image afterwards.

In this paper we give a full description of the algorithm, as well as the results obtained from its application to data from the two ESA SPectra bARrax Campaigns (SPARC)[21]. In-situ reflectance measurements taken simultaneously to CHRIS/PROBA acquisition have been used in the validation of the atmospherically corrected data, finding a good agreement. Moreover, some analysis of the directional features in the reflectance of several targets will be performed, in order to show the potential of CHRIS/PROBA data for monitoring Earth's surface processes.

Moreover, a prototype of an atmospheric correction method for inland waters is being designed too. The description of its current state is also given in the paper. The first results of water leaving reflectance are encouraging, after comparison with in-situ measurements.

2. METHODOLOGY FOR LAND TARGETS

2.1. Fundamental basis

The algorithm is based on the combination of principles of the empirical line and the radiative transfer approaches: an empirical line-like procedure is used to calculate an updated set of CHRIS's gain coefficients for the radiance measurements, while a common radiative transfer approach is followed after in order to retrieve surface reflectance from TOA radiances.

It must be remarked that the calibration coefficients do not provide surface reflectance, as it would be the case of an empirical line method, but are only used to correct the mis-calibration trends found in the radiance measurements. Thus, the similarity of the algorithm presented in this work with standard empirical line methods is the derivation of linear correlations from several pixels with some spectral contrast to find calibration coefficients, but these are not used to retrieve surface reflectance here. For the retrieval of this surface reflectance, AOT and water vapor content estimated jointly with the calibration coefficients are used as an input in a radiative transfer code to calculate the atmospheric optical parameters for the 5 angular configurations of CHRIS/PROBA acquisitions.

For those estimations, the atmospheric state is considered invariant within the area covered by the image, which is quite realistic for CHRIS/PROBA images, approximately square with a swath around 15 km. Surface reflectance is expressed as a linear combination of two vegetation and soil spectra, which act as artificial endmembers. Then, aerosol and water vapor contents, as well as the abundances of vegetation and soil, are retrieved simultaneously from 5 pixels inside the image, by means of a multiparameter inversion of the TOA spectral radiances

One might think that a better strategy would be performing an iterative procedure in which the calibration coefficients are calculated firstly, and the retrieval of atmospheric parameters is done using the calibrated radiances as a second step of the method. However, since coefficients and atmospheric parameters are calculated jointly at first, they are slightly coupled. This means that there

would not be much difference between the atmospheric parameters retrieved in both steps, increasing the computation time in addition.

2.2. Inversion procedure

The inversion is performed by minimizing a Merit Function δ^2 specifically designed for this problem,

$$\delta^2 = \sum_{pix=1}^5 \sum_{\lambda_i} \frac{1}{\lambda_i^2} [L^{SEN}|_{pix,\lambda_i} - L^{SIM}|_{pix,\lambda_i}]^2 \quad (1)$$

where L^{SIM} is the TOA radiance simulated with the radiative transfer code, λ_i corresponds to the center of the i band, given in μm units, in the particular band configuration of the sensor, and L^{SEN} stands for the TOA radiance measured by the sensor. The equivalent TOA apparent reflectance ρ^{SEN} is given in terms of the TOA radiance, the solar constant E_{sc} and the cosine of the solar zenith μ_s angle by

$$\rho^{SEN} = \frac{\pi L^{SEN}}{\mu_s E_{sc}}. \quad (2)$$

The Merit Function in Eq. 1 is weighted by λ_i^{-2} to drive the inversion towards the smaller wavelengths, where the effect of the aerosols is bigger, while the reflectance of most of the natural surfaces is lower.

For aerosol characterization, the Standard Radiation Atmosphere (SRA) types defined by the Radiation Commission of the International Association of Meteorology and Atmospheric Physics (IAMAP) [22], dust-like, water soluble, oceanic and soot, are implemented in the 6S database. So, aerosols are specified by means of the AOT at 550 nm and the percentages of those basic types, resulting in 4 parameters. Thus, the free parameters to be calculated in the optimization are the water vapor column content, the aerosol optical thickness at 550 nm and the percentages of basic types, and the proportions of vegetation and soil for each of the 5 reference pixels.

The 6S (Second Simulation of the Satellite Signal in the Solar Spectrum) radiative transfer code [23] was chosen for the atmospheric simulations. The MODTRAN4 code [24], instead of 6S, is generally used in such hyperspectral processing, because of the rigorous treatment of scattering and absorption processes in the radiative transfer simulations, the accurate coupling between the atmosphere and the directional properties of surface reflectance, and its high spectral resolution of up to 1 cm^{-1} . However, the much faster 6S code was chosen, since the accuracy differences between the codes can be neglected when compared with the commented calibration problems.

For the CHRIS Mode-1 band configuration, the bands inside the oxygen-A absorption band are not considered, due to the difficulties in the computation of such a narrow and strong absorption. Moreover, CHRIS presents some calibration problems in the extremes of the detector focal plane array. The first band is also discarded, and the same is done for wavelengths larger than $0.9 \mu\text{m}$.

The 5 reference pixels must have as spectral contrast as possible (ranging from pixels with high green vegetation content to high bare soil content) in order to find a maximum sampling for the linear correlation in the calculation of calibration coefficients, with low and high radiance points. Moreover, the spectral contrast is helpful to achieve a maximal decoupling between atmosphere and surface contributions to TOA signal. A perfect choice for the set of reference pixels would be a pure vegetation pixel, a pure bare soil pixel, and three intermediate ones, mixture of vegetation and soil. The particular selection of 5 as the number of pixels to serve as a reference for the retrievals is a balance between the computation burden and the number of points for the calculation of the coefficients: a higher number would increase the computation time, without adding too much information to the sampling. In the operative procedure, the selection is based on the definition of three categories of land pixels, using the *Normalized Difference Vegetation Index* (NDVI) [25] calculated from TOA reflectances. Pure bare soil pixels are those with a NDVI value between 0.01 and 0.1, mixed pixels are between 0.1 and 0.45, and pure vegetation pixels have a NDVI in the range 0.45–0.7. To assure a maximum spatial sampling within the window, the reference pixels are selected randomly from each one of the categories.

For the construction of the simulated TOA radiance L^{SIM} , CHRIS bands are reproduced using Gaussian filter functions, even though the binning (superposition of several narrow bands to constitute a band with the increased width) in the shorter wavelengths makes the shape more rectangular. The surface is assumed to be Lambertian, what leads to the expression

$$L_{SIM}(\mu_s, \mu_v, \phi) = t_g \left[L_0 + \frac{\pi}{\mu_s E_{sc}} \frac{T \uparrow T \downarrow \rho_s}{1 - S \rho_s} \right], \quad (3)$$

where t_g is the transmittance due to gases; L_0 is the intrinsic atmospheric radiance, also called atmospheric path radiance; ρ_s is the surface reflectance; S is the spherical albedo, reflectance of the atmosphere for isotropic light entering it from the surface; μ_v is the cosine of the view zenith angle; ϕ is the relative azimuth between the Sun and viewing directions; $T \uparrow$, $T \downarrow$ are, respectively, the upward and downward total atmospheric transmittances (for diffuse + direct radiation), in the illumination and observation directions. The angular dependencies of t_g , L_0 , $T \uparrow$ and $T \downarrow$ have been omitted for the sake of simplicity.

The surface spectral reflectance is given by the linear combination of two artificial endmembers of typical green vegetation and soil spectra,

$$\rho_s = C_v \rho_{veg} + C_s \rho_{soil} \quad C_{v,s} > 0, \rho_s \in [0, 1] \quad (4)$$

The proportions of vegetation and soil are allowed to be larger than 1.0 in case spectra brighter than the endmembers were present. The 10 coefficients $C_{v,s}$, 2 for each of the 5 pixels, are also free parameters in the TOA radiance simulation. The endmembers' role is to provide a reflectance-basis for the construction of TOA radiances, but not reproducing real targets present in the scene. That is why the term "artificial" is used. As a result, the $C_{v,s}$

coefficients are not real abundances, but effective abundances of the endmembers. The ideal case would be the availability of an algorithm for the estimation of endmembers free from the atmospheric influence, but no one has been found. Anyway, the hypothesis that any common land pixel can be represented by this kind of linear combination seems to work well in the reduced spectral range covered by CHRIS, where most of the target's specific absorption/reflectance characteristic features can not be identified. Further effort will be needed for the extension of the method to sensors covering the 0.4–2.5 μm range.

Neglecting the directional effects in the target reflectance provides a simple formulation of the radiative transfer, what leads to an important decrease in the computation time and modelling effort. It has been demonstrated that the Lambertian approach can work well in the general case where the acquisition geometry is not in the retro-dispersion hot spot direction [26], and so if the observation is close to nadir. Thome et al.[27] state that the percentage difference between the Lambertian case and typical non-Lambertian cases is less than 1% in the near nadir viewing range. So, in order to reduce the errors associated to this approach, the atmospheric retrievals are performed from the image acquired from the view zenith angle closer to nadir (in PROBA nomenclature, FZA equals to 0°), and the corresponding atmospheric transmittance and reflectance functions in Eq. 3 needed to derive the surface reflectance are calculated then for each one of the 5 acquisition geometries. In any case, the $C_{v,s}$ coefficients partially account for directional properties, as the effective abundances of vegetation and soil they represent vary with the observation angle.

The minimization of the Merit Function in Eq. 1 is performed by the Powell's Minimization Method [28], based on a 1-D minimization separately in each direction of the parameters space, without the need for the analytical expression of the function derivatives. An appropriate initialization of the Powell's algorithm is needed in order to reduce the convergence time and to reach the best minimum. Default climatology values are used for the atmospheric species, while a strong correlation between the NDVI and the coefficients $C_{v,s}$ was found from several simulations.

2.3. Calculation of calibration coefficients

Once the minimization of the Merit Function has been performed, the resulting modelled and real TOA spectra are used in order to derive the calibration coefficients in each of the CHRIS bands. Since fails in CHRIS calibration are expected to happen in the gain coefficients, rather than in the dark current, a linear regression with the intercept set to 0 is considered,

$$L_i^{SIM} = A_i L_i^{SEN} \quad (5)$$

being A_i the updated calibration coefficient for the TOA radiance in the channel i th. The 5 points obtained from the 5 reference pixels are fitted by means of a least squares algorithm. With the aim of discriminating those pixels where the assumption of the linear correlation

worked worst, the linear regression is weighted with a CHI square value accounting for the goodness of the fit.

In this way, a set of A_i coefficients is calculated from the CHRIS/PROBA image acquired with the minimum VZA. Since calibration coefficients are intrinsic to the sensor, and not angle-dependent, the same set of coefficients is applied to the 5 images acquired from 5 angles in the same overpass. The validity of this assumption will be shown later.

2.4. Surface reflectance retrieval

Once the calibration coefficients are obtained, the 5 TOA radiance images provided by the sensor are re-calibrated. After, the calculated atmospheric functions are used to retrieve the surface reflectance images. As a starting point, a Lambertian reflectance for the surface is assumed, what leads to the analytical inversion of Eq. 3 to retrieve ρ_s . An initial surface reflectance image is obtained with a little algebra.

This is an important justification for the Lambertian assumption. However, some authors have pointed out that this approach may lead to noticeable errors in some particular combinations of geometry, target reflectance and atmospheric conditions [29, 30]. The problem is that multiangular information is needed in order to characterize properly the directional effects in the target. In the case of platforms with multiangular viewing capabilities, such as PROBA, accounting for the directional effects in the target reflectance is feasible.

Then, although the general procedure is based on the Lambertian assumption also for CHRIS/PROBA, a further step involving directional effects was been done for some pixels in the image. It performs an iterative scheme, in which directional effects are corrected in each of the steps. A detailed description of the procedure is given in [31]. It has not been implemented in the operational algorithm because of several reasons, such as the prohibitive computation time, the error associated to the geometric correction or the low overlapping proportion found for the 5 CHRIS/PROBA images in some dates. However, tests have been made for some pixels in the CHRIS/PROBA images, extracted visually from the center of some targets (alfalfa, corn and bare soil) in the overlapped region, to avoid the problems with the geometric correction. Results for these sample show that the errors arisen with the Lambertian approach are smaller than a 8% in the worst cases, FZA= $\pm 55^\circ$ and corn crop. In the other angles, FZA= $0^\circ, \pm 36^\circ$, the average errors are around a 3%. Although those results justify the Lambertian assumption considered here, a more intensive analysis of the directional effects in the atmospheric correction of CHRIS/PROBA data should be done using a larger data set, covering a wide range of solar zenith angles and relative azimuth positions, in order to assess to what extent directional effects must be considered in the atmospheric correction of multiangular data.

The final step in our atmospheric correction algorithm is the removal of the image blurring caused by those photons reflected by the target environment and scattered by

the atmosphere particles into the sensor's line-of-sight. This effect is called *adjacency effect*, because the apparent signal at the TOA for a given pixel comes also from the adjacent ones.

We follow the simple formulation proposed by Vermote et al. [29], which is based on the idea of weighting the strength of the adjacency effect by the ratio of diffuse to direct ground-to-sensor transmittance:

$$\rho_s = \rho_s^u + \frac{t_d(\mu_v)}{e^{-\tau/\mu_v}} [\rho_s^u - \bar{\rho}^u], \quad (6)$$

where ρ_s the final surface reflectance, ρ_s^u is the surface reflectance before the adjacency treatment, output of the complete atmospheric correction algorithm, $t_d(\mu_v)$, $e^{-\tau/\mu_v}$ the transmittances for diffuse and direct radiation in the ground to sensor path, and $\bar{\rho}^u$ is the average of the environment reflectance. This average is calculated for a $1 \times 1 \text{ km}^2$, which is in the same order of the aerosol coupling scale. In the present case of CHRIS Mode-1, this means a window of around 30×30 pixels.

A flow chart describing the whole atmospheric correction process is displayed in Fig. 2. Summarizing, it starts with the extraction of the 5 reference pixels from the FZA= 0° image, which is made according to an initial classification of candidate pixels based on NDVI thresholds. The AOT, water vapor content and calibration coefficients are retrieved simultaneously by means of the inversion of the TOA radiances in the 5 reference pixels. The coefficients are used to update the radiance values in the set of 5 images acquired in the same CHRIS/PROBA overpass, while AOT and water vapor are inputs in the calculation of the atmospheric optical parameters for the 5 angular configurations. The analytical inversion of Eq. 3 and the removal of adjacency effects are the last steps in the retrieval of the final surface reflectance images.

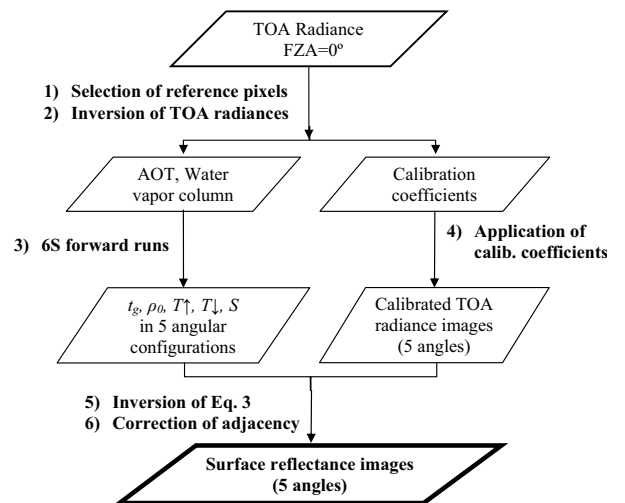


Figure 2. Flow chart describing the main steps for the surface reflectance retrieval.

3. METHODOLOGY FOR INLAND WATERS TARGETS

In the case of inland waters pixels, the particular performance of CHRIS in the Mode-2 configuration (optimized for the observation of water bodies) makes a different approach must be followed in the retrieval of the atmospheric parameters. Concretely, the use of land pixels should be avoided for Mode-2 data [20], due to the saturation found for surface albedos higher than around 25%. Thus, the methodology discussed previously for Mode-1 is not applicable to Mode-2 data.

According to the particular spectral response of water targets, characterized by very low reflectances in the NIR wavelengths, the water vapor absorption feature centered around 940 nm cannot be used to estimate the atmospheric water vapor content. However, since the water vapor absorption is only residual in the rest of the spectral range covered by CHRIS, we shall assume a default value for the integrated column. Neglecting water vapor variations is not a critical issue, since Mode-2 channels are located in wavelengths out of water vapor absorptions.

For aerosols, the situation is completely different, as their influence on the radiation is maximum in the visible region, where most of the absorption features due to water pigments happen. The main idea is to perform an iterative procedure that seeks for the AOT that minimizes the subsequent water reflectance in CHRIS bands 2 and 3 (centered around 440 and 490 nm), where the aerosol scattering is maximal, with the physical constraint that the reflectance has to be positive. The first band, centered in 410 nm, is avoided because of the high noise levels detected. No re-calibration procedure is needed for this Mode-2: because the ratio signal-to-noise is low in the NIR bands, no mis-calibration can be detected in them. The pixel used for the inversion is a representative pixel selected from the middle of the reservoir. The use of clusters of pixels is foreseen for future versions of the method, to account for instabilities caused by noise in the instrument or fluctuations in water composition.

Once the AOT has been estimated, the surface reflectance images are obtained from TOA radiance ones using the procedure described in section 2.4. First results of this methodology are shown in section 5.

4. RESULTS FOR LAND TARGETS

4.1. CHRIS/PROBA Data Available from SPARC campaigns

The SPARC campaigns [21] were held in the Barrax (39.05°N, 2.10°W, La Mancha, Spain) CHRIS/PROBA core site in July 2003 and 2004, as part of the Phase-A Preparations for the Surface Processes and Ecosystem Changes Through Response Analysis (SPECTRA) mission [32]. The Barrax site is a flat continental area with an average elevation over the sea level of around 700 m. There is a big contrast in natural surfaces, ranging from large homogeneous vegetation fields (e.g. alfalfa

and potatoes crops) to large dry bare soils. The crops in the area were classified previously, so the comparison between in-situ surface reflectance measurements and the atmospherically corrected data is feasible for different land uses.

Four CHRIS/PROBA data sets over the Barrax area are available (acquired in Mode-1, 62 bands and 34 m spatial resolution), two for each year. For the SPARC 2003 campaign, acquisitions were made on the 12th and the 14th July. The situation over Barrax on those days was particularly favorable, because PROBA almost passed over (-4° across-track zenith angle) on 13th July, and then on the 12th July (+20° across-track zenith angle) and on 14th July (-27° across-track zenith angle). Unfortunately, the image from 13th July was not correctly taken because of satellite pointing problems, so we have had only two images from the campaign. Concerning SPARC 2004, two data sets were also acquired, on 15th and 16th July. Nevertheless, the system failed on the first date, and only 3 of the 5 images for 15th July were recorded. The observation angles for each of the two days and the two years are plotted in Fig. 3. It must be remarked that all the images have been initially corrected from drop-outs and striping in the first pre-processing step, and geometrically corrected afterwards.

Despite the failures in the acquisitions, the resulting data base, with 4 different dates, turned out to be enough for the validation exercise, as well as to show the capabilities of the CHRIS/PROBA data to represent the particular spectral and angular features of different targets. The results obtained from the application of the algorithm to those images and the validation with in-situ measurements will be discussed next.

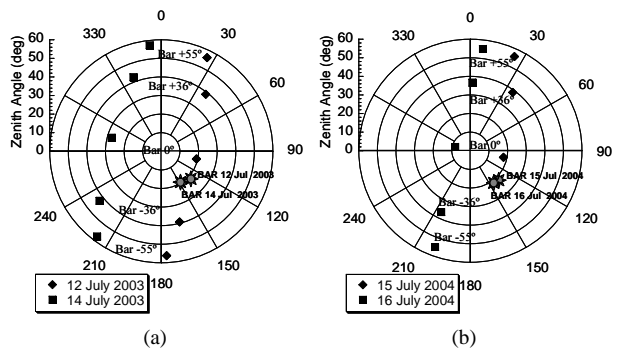


Figure 3. Acquisition geometries and illumination angles for the images of (a) SPARC 2003, and (b) SPARC 2004. Labels indicate the corresponding nominal FZA of the closest symbols.

4.2. Inversion of TOA radiances and retrieval of calibration coefficients

Starting with the inversion of TOA radiances, Fig. 4 shows the fits obtained by the minimization of the Merit Function in Eq. 1, for 2 of the 5 selected reference pixels in the image from the 12th July 2003. It may be noted that, although there is a general overlapping between the

TOA CHRIS/PROBA radiance spectra and the modelled curves, noticeable discrepancies exist in some bands.

Dashed circles show the wavelengths where the disagreement is a maximum. The bands in the edges of the spectral range are among them. The first band presents important noise levels, as expected in those channels in the extremes of sensors compounded of focal planes arrays. Some spikes appear around $0.5 \mu\text{m}$, what might be explained by a possible spectral shift in the band center wavelengths in such spectral region, or by the abrupt transition caused by the different number of CCD rows integrated in bands 6 (5 CCD rows) and 7 (4 rows) [20]. Finally, the NIR region is affected by a systematic overestimation of the TOA signal, as it can be checked by comparing with the simulated spectra. Similar trends are found in the rest of data sets, both in 2003 and 2004.

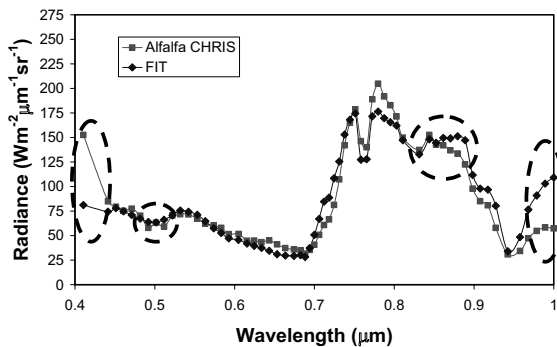


Figure 4. Fit of 1 of the 5 reference pixels for the derivation of the calibration coefficients, as well as aerosols and water vapor retrieval, corresponding to the FZA = 0° image of 12 July 2003. Dashed circles point the wavelengths with major deviations.

The resulting A_i coefficients calculated from the 4 dates of CHRIS/PROBA acquisitions are plotted in Fig. 5. A good agreement is observed. The largest deviations are found in the wavelengths centered around $0.94 \mu\text{m}$, what might be explained by the important perturbation due to water vapor. However, some degradation in the instrument seems to have been found in addition, because the shapes of the curves are coincident by pairs, with similar trends in the dates corresponding to the same year, either 2003 or 2004. Anyway, the temporal stability of CHRIS gain factors has been assessed to a large extent, which is a good proof on the instrument reliability, despite the fact that the CHRIS/PROBA system was launched only for technology demonstration purposes.

Moreover, the calibration is more important in the NIR wavelengths, with coefficients reaching a factor 2. The correction in the first band is important as well. This confirms the a priori expectations, because the focal plane array is designed to have the best radiometric quality in the central wavelengths, getting worse as the wavelength approaches both edges of the spectral domain. Besides, the underestimation in the measurements in the NIR wavelengths is detected and corrected here. Both the general shape and the levels of the recalibration curve are in very good agreement with the one provided by Sira Technology Ltd, the company on charge of the design of the instrument, calculated from engineering arguments [19],

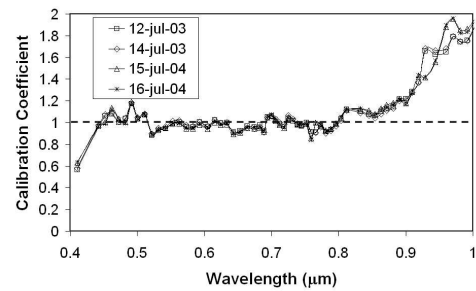


Figure 5. Calibration coefficients A_i calculated for the 4 dates of CHRIS/PROBA SPARC acquisitions.

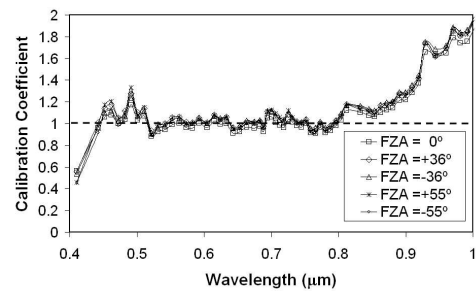


Figure 6. Calibration coefficients calculated for the 5 angles of the same overpass on the 12th July 2003.

which confirms the good performance of the methodology presented here.

Even though the calibration coefficients are retrieved from the image acquired from the minimum VZA, FZA = 0° , and applied to the rest of angles afterwards, the robustness of the calculated coefficients to angular variations must be checked. The sets of coefficients calculated independently from the 5 angles in the overpass on the 12th July 2003 are displayed in Fig. 6. It can be seen that the calibration curves are nearly angle-independent, as the different curves are almost overlapped. This reinforces the validity of the coefficients as universal coefficients to be applied in a vicarious calibration of the raw TOA data.

Regarding the retrieval of atmospheric parameters, water vapor contents of 1.11, 1.23, 1.52 and 1.68 gcm^{-2} were obtained for the 12th and 14th 2003 and the 15th and 16th 2004, respectively. There is a high correlation with the 1.4, 1.6, 1.9 and 2.1 gcm^{-2} values measured by radiosoundings launched simultaneously to PROBA overpasses in both campaigns. However, it is difficult to achieve a better accuracy due to the remarked mis-calibration. The most important thing here is that these values are consistent with the calibration coefficients calculated simultaneously, what is needed to lead to reliable values of the subsequent surface reflectance. Common values of 0.2, 0.25, 0.17 and 0.28 were calculated for the AOT at 550 nm in the same dates.

4.3. Results for surface reflectance

The surface reflectance after the complete atmospheric correction for several pixels is shown in Fig. 7, altogether with field measurements. The in-situ reflectance measurements were taken with an Analytical Spectral Devices (ASD) FieldSpec Pro FR Spectroradiometer (footprint around 0.8 m, 2 nm of spectral resolution). These measurements were acquired almost simultaneously to satellite overpasses (time differences were always smaller than 30 minutes) from a nadir view while walking across the target, integrating in one spectrum all the measurements taken for every path of around 10 m. The reason for this is assuring that most of the natural variability in the target could be reproduced. The grey stripe gives the mean value and the standard deviation calculated from all the acquisitions made for the same target, to provide information on the spatial variability of the target.

The agreement between the ASD spectroradiometer and CHRIS data is relatively good, both in the shape and in the reflectance levels, what validates the methodology presented here. It must be taken into account that the field spectra were acquired from a nadir view, not coincident with any of the PROBA view angles, so small deviations due to angular trends are expected a priori. This is confirmed by the fact that the maximum agreement with the in-situ measurements is found for the minimum view zenith angle. Thus, since we are comparing different observation angles, a detailed error study has not been done, considering the visual comparison enough in order to check the good performance of the atmospheric correction method. The fit of the resultant multiangular surface reflectance information to a parametric reflectance model can provide the necessary interpolation to the nadir view for an accurate statistical analysis.

Nevertheless, it can be stated that the comparison is fairly good in the case of the uniform Lambertian alfalfa targets, and also for the sunflowers crop. In this case, though, a large natural variation was found, due to the crops consisted of plant rows separated by bare soil. The agreement reinforces the integrating procedure used in the ground measurements. For bare soils the directional effects are more important, what makes larger deviations are found in some targets. Finally, the bad comparison with the dry wheat crop might be explained by the practical difficulties in the measurement process, arisen because of the density and height of the plants.

Surface reflectances for the 5 views of the same point in 4 different targets are plotted in Fig. 8. An accurate analysis of the directional effects appearing in those plots is out of the scope of this work, but some expected features can be noticed easily. It can be stated that the magnitude of the directional effects varies with the nature and vertical structure of the target, according to the behavior predicted by the radiative transfer theory. In order to quantify those angular differences, a function δ_i is defined as the standard deviation σ_i of the surface reflectance in the 5 angles for the i channel, normalized by the mean value ρ_{s_i} :

$$\delta_i = \frac{\sigma_i}{\rho_{s_i}} \quad (7)$$

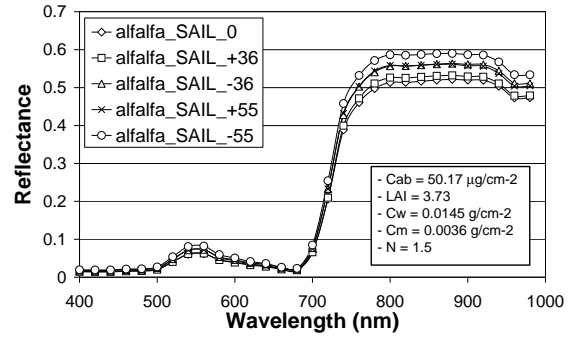


Figure 9. Results of SAIL/PROSPECT simulations using in-situ measurements of the biological parameters for the alfalfa crop and the geometrical configuration plotted in Fig. 3.

According to δ_i the alfalfa crop, consisting of uniform dense short canopies, is closer to the Lambertian behavior than the vertical tall (around 2 m height) corn canopy, where the angular effects are more important. Calculating the mean values of δ for two spectral regions, in the red (10 bands, from 604 to 688 nm) and in the NIR (10 bands, from 804 to 900 nm), we obtain $\delta_{red} = 0.10$ and $\delta_{NIR} = 0.06$ for the alfalfa, while $\delta_{red} = 0.15$, $\delta_{NIR} = 0.10$ for the corn. Something similar occurs between the bare soil and the dry wheat targets: although the spectral response is quite similar, directional effects are more intense in bare soils, as the wheat cover consists of a very dense canopy, almost uniform, that tends to make isotropic the angular response due to multiple scattering processes ($\delta_{red} = 0.08$ and $\delta_{NIR} = 0.05$ for the wheat, while $\delta_{red} = 0.12$, $\delta_{NIR} = 0.09$ for the soil).

Since no in-situ multiangular measurements were available, the consistency of the directional behavior registered by the CHRIS/PROBA data has been checked using a newer coupled version of the SAIL and PROSPECT models [33] for simulating the reflectance of a real alfalfa crop. We have selected the alfalfa crop because of its 2-D uniformity, what makes it the prototype of crop to be modelled with the SAIL/PROSPECT model. Besides, all the inputs needed (chlorophyll content, LAI, water content and dry matter content) were explicitly measured during the SPARC 2004 campaign. Results for the 5 angles in Fig. 3 are plotted in Fig. 9. The input values for the model are shown in the legend. It can be stated that both the spectral shape (Fig. 9) and the angular dependencies (Fig. 10) are highly coincident with those showed for the alfalfa crop in Fig. 8, what confirms the validity of the procedure described in this work, as well as the potential of CHRIS/PROBA to reproduce the reflectance trends of real surface, both in the spectral and angular domains.

5. RESULTS FOR INLAND WATERS TARGETS

CHRIS/PROBA Mode-2 images acquired over the Rosarito reservoir, located in Northern Spain (40.12°N, 5.27°W) have been used in this study. Results obtained from the atmospheric correction of the image of 20 May 2004 are shown in Fig. 12. The acquisition angles for

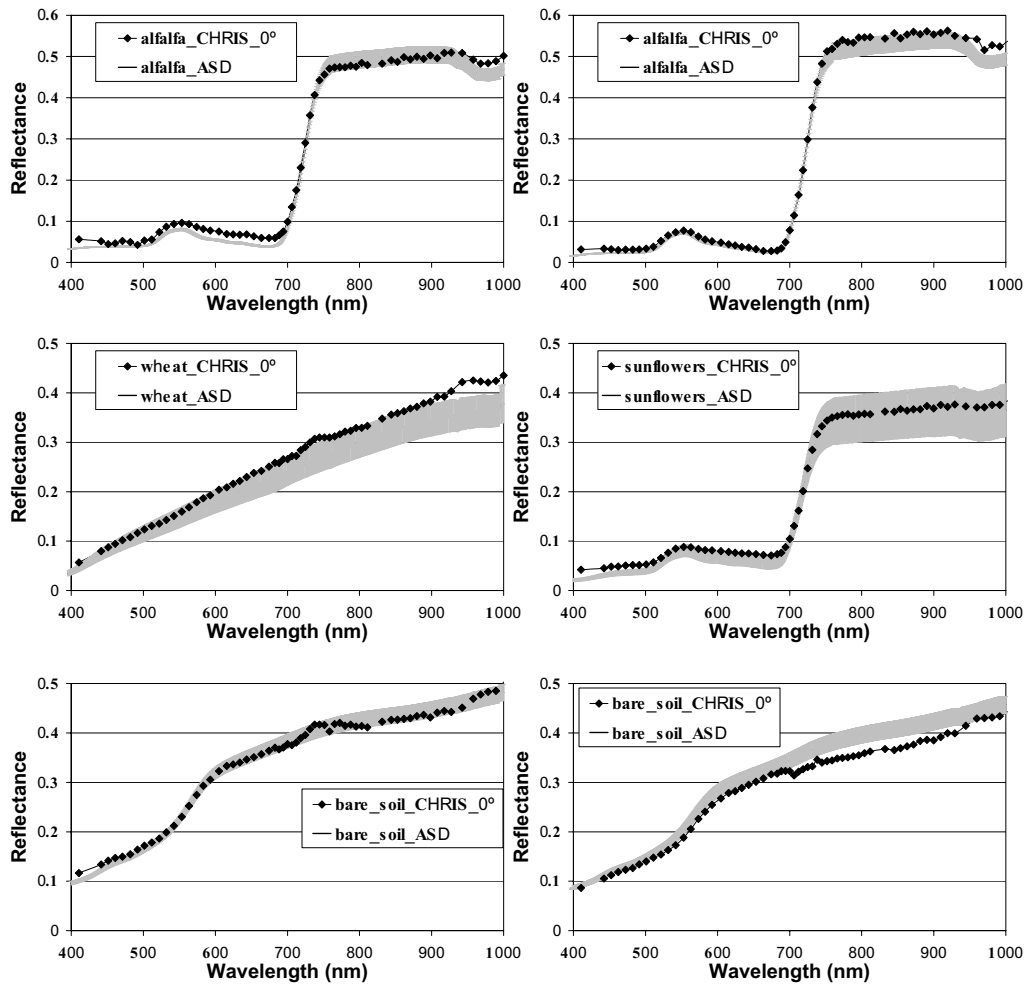


Figure 7. Sample surface reflectance spectra for different targets, compared with in-situ measurements taken with an ASD spectroradiometer. Plots in the left column come from SPARC 2003 data, and those in the right one from 2004.

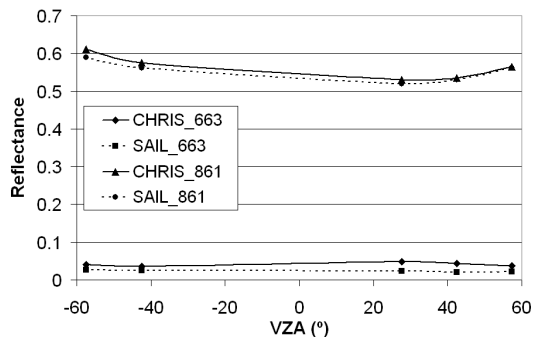


Figure 10. Projection of the alfalfa simulations in Fig. 9 on the view zenith angle (VZA), for 2 wavelengths in the red (663 nm) and in the NIR (861 nm) regions.

this date are plotted in Fig. 11. The 5 views of the same point in the Rosarito reservoir and the corresponding in-situ reflectance spectrum measured simultaneously to the CHRIS/PROBA acquisition are plotted. In-situ measurements come from the Spanish Center for Hydrographic Studies (CEDEX), in the frame of its activities to validate algorithms for the monitoring of water quality using remote sensing data [34].

It has to be remarked the relatively high agreement between CHRIS data and the in-situ spectrum, taking into account the low signal arriving at the sensor from water targets and that the field measurement angle is not coincident with any of the CHRIS/PROBA observation angles. Nevertheless, the closest spectrum to the nadir-ASD measurement is again corresponding to the minimum VZA, as expected. This validates both the quality of CHRIS Mode-2 data and the aerosol retrieval and atmospheric correction procedures implemented for inland waters.

On the other hand, the large directional behavior expected for water bodies is found in CHRIS/PROBA data: even though acquisition angles are not in the principal solar plane, forward and backward scattering regions can be

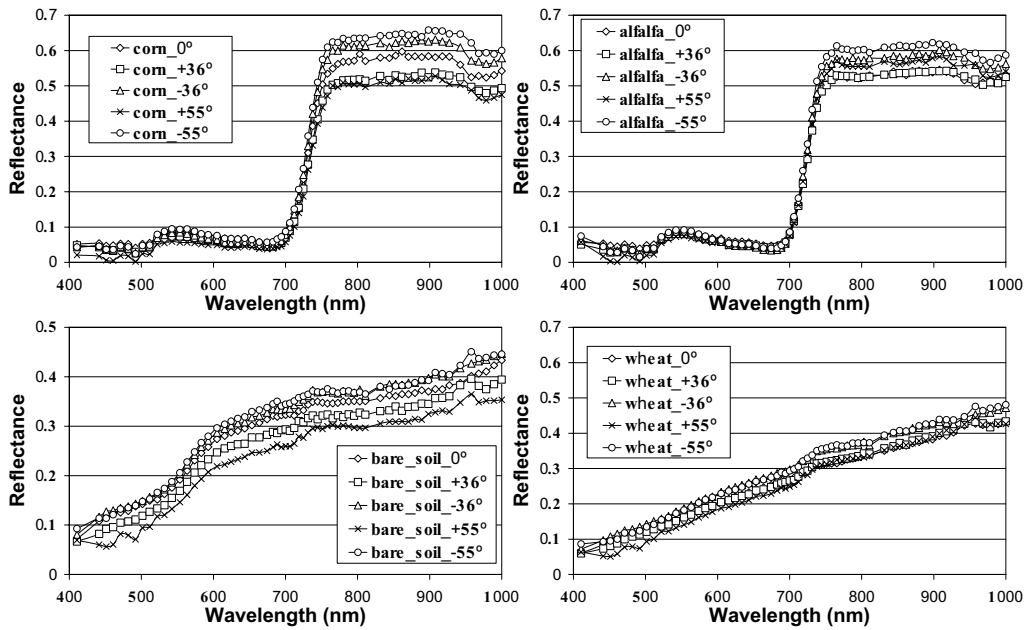


Figure 8. Composition of surface reflectances from different targets for the 5 different CHRIS/PROBA acquisition angles.

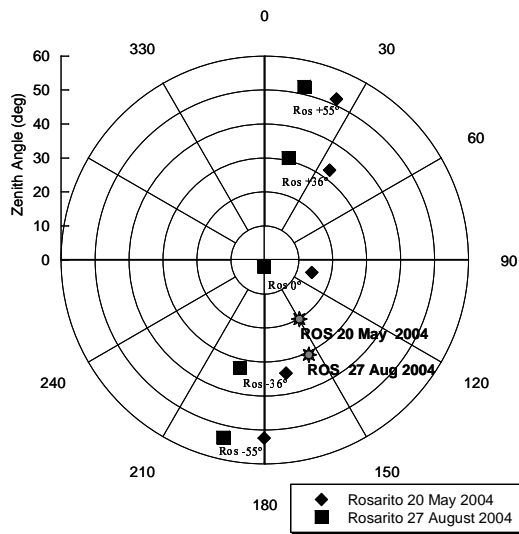


Figure 11. Acquisition angles for two sets of Rosarito images.

clearly predicted in Fig. 11. The maximum reflectance should be expected in the specular reflection region, typical in polished surfaces such as calm water bodies. The closest angle to the ideal specular position in the geometrical configuration of the Rosarito scene of 20 May 2004 is the one labelled by “+36”. The maximum of reflectance for this angle can be observed in Fig. 12.

Moreover, the angular dependency of the registered reflectance can be found not only in the mean reflectance value, but also in the composition variability inside the reservoir. While the Rosarito reservoir looks very uniform when viewed from one direction, noticeable structures with different tonalities can be seen when it is observed from another one. An example is displayed in

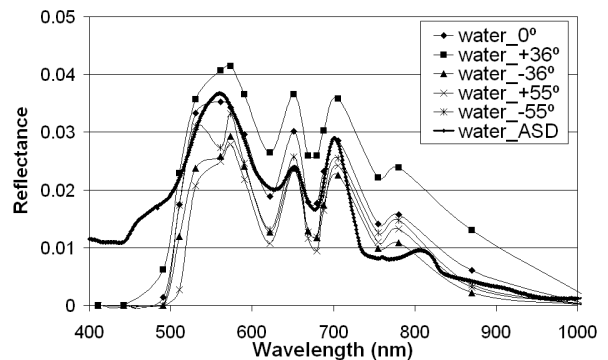


Figure 12. Comparison of CHRIS water reflectance spectra for the 5 different observation angles plotted in Fig. 11 with an in-situ measurement acquired simultaneously on 20 May 2004.

Fig. 13, for the “+36” and “-36” angles. Several spectra have been extracted randomly from all over the reservoir. Large differences can be detected in the “+36” angle, while the “-36” appears as much more uniform. Therefore, one observation angle may turn out to be more useful than the other with the aim of water quality analysis. Besides, multiangular information is very useful in the substitution of those pixels mostly affected by the sunglint effect in any of the observation angles.

6. CONCLUSIONS

Two different methodologies for the atmospheric correction of CHRIS/PROBA data have been presented. A major part of the paper has been devoted to the description of an atmospheric correction of CHRIS/PROBA data over land. In addition, the current state of an atmospheric cor-

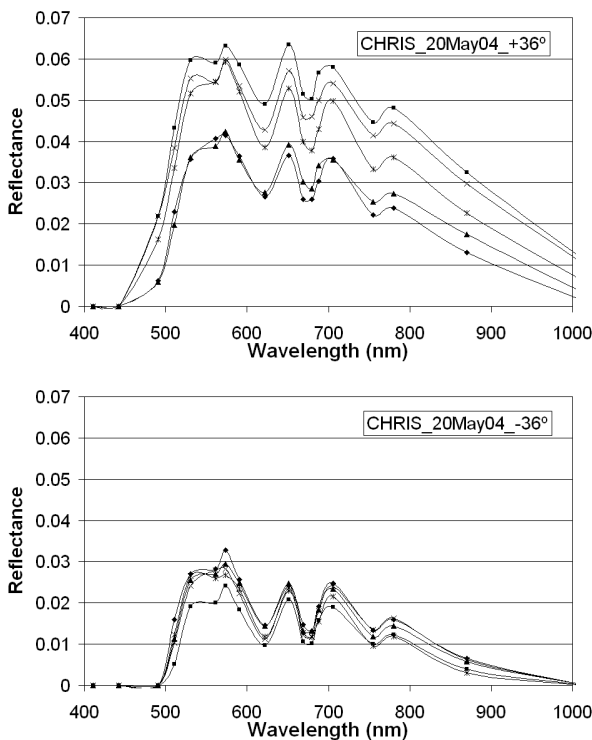


Figure 13. Sample of Rosarito reflectance spectra, extracted randomly for different pixels across the image, for two different observation angles.

rection algorithm for the atmospheric correction of inland waters targets has also been described.

Concerning the atmospheric correction algorithm for CHRIS/PROBA data taken over land, a detailed description of the algorithm steps has been introduced in this work, as well as the results obtained from its application to CHRIS/PROBA data from the SPARC 2003 and 2004 campaigns. The performance of the method has been assessed using in-situ measurements from those campaigns.

Since important calibration problems have been reported in several CHRIS channels for 2003 and 2004 data, a standard radiative transfer approach to the atmospheric correction can not be applied. Indeed, any processing methodology for CHRIS/PROBA should deal with the update of CHRIS gain coefficients as an important issue. The method presented in this work retrieves simultaneously a set of calibration coefficients and the atmospheric optical parameters for the 5 acquisition geometries. It works in a fully automatic way, without the need for any ancillary data, neither atmospheric parameters nor surface reflectance.

The algorithm's fundamental basis lies on the inversion of the TOA radiances from 5 reference pixels with a high spectral contrast. The 5 fits of modelled radiances to real ones are used to calculate the calibration coefficients, by means of the linear regression of the resulting 5 points in each spectral band. The AOT and water vapor column content are also retrieved in the inversion. Those con-

tents are the inputs to the radiative transfer code in the calculation of the atmospheric optical parameters for the 5 CHRIS/PROBA acquisition geometries. The spectral contrast of the reference pixels allows the separation of atmosphere and surface contributions to TOA radiances, as well as a proper sampling of radiances to calculate the calibration coefficients. Once the 5 TOA radiance images are calibrated, surface reflectance is obtained from them using the calculated atmospheric parameters in the 5 angular configurations. Finally, adjacency effects are removed from the images.

The calculated sets of calibration coefficients showed the high temporal stability of the instrument, without too much variation in the response between 2003 and 2004 years. Moreover, the spectral shape of the derived curves compares very well with the one calculated from engineering assumptions by CHRIS operators, which enhances the reliability of the presented methodology. Finally, the robustness to angular variations in the retrieved coefficients is also a good sign of the method consistency.

Concerning surface reflectance retrievals, SPARC 2003 and 2004 data have been used to validate the method. Reflectance field spectra acquired with a spectroradiometer have been compared with CHRIS/PROBA atmospherically corrected data, showing a good agreement both in the spectral shape and the reflectance levels, although small deviations because of different observation angles are expected. The capability of CHRIS/PROBA data to reproduce the directional properties of a vegetation crop has also been assessed. Due to the absence of multiangular field measurements, those have been simulated by means of a coupled version of the PROSPECT and SAIL models. Real data of the needed biophysical variables have been used as an input, leading to a good agreement with CHRIS/PROBA results.

The potential of CHRIS/PROBA to reproduce real spectral and angular trends in land targets has been shown, as long as the appropriate processing techniques are used. Nevertheless, further analysis of the limitations of the Lambertian approach in the atmospheric correction of CHRIS/PROBA data is foreseen. Also, the application of the method to the analysis of the quality of 2005 data, in which the instrument's spectral calibration issue has been revisited.

Finally, with respect to inland waters targets, a short description of the algorithm which is under development has been given. First results from the processing of one date of acquisition are shown. The comparison with in-situ measurements of water-leaving reflectance are promising, although further validation with other data sets is still needed.

ACKNOWLEDGMENT

This work has been done in the frame of the ESA-SPARC Project, contract ESTEC-18307/04/NL/FF. The first author (LG) acknowledges the support by a PhD grant from the Spanish Government, Ministry of Education and Science. The authors also want to thank M. Cutter from Sira

Technology Ltd. for his assistance with CHRIS technical issues, and to R. Peña, J. A. Domínguez and A. Verdú for the provision of inland waters data.

REFERENCES

- [1] Barnsley, M. J., Settle, J. J., Cutter, M., Lobb, D., and Teston, F. The PROBA/CHRIS mission: a low-cost smallsat for hyperspectral, multi-angle, observations of the earth surface and atmosphere. *IEEE Trans. Geosci. Remote Sens.*, 42:1512–1520, 2004.
- [2] Fraser, R. S. Computed atmospheric corrections for satellite data. In *Conf. Scanners and Imagery Systems for Earth Resources Observations, Proc. SPIE*, volume 51, 1974.
- [3] Kaufman, Y. J. The atmospheric effect on remote sensing and its correction. In Asrar, G., editor, *Theory and Applications of optical Remote Sensing*, pages 336–428. Wiley and Sons, New York, 1989.
- [4] Green, R., Eastwood, M., Sarture, C., Chrien, T., Aronsson, M., Chippendale, B., Faust, J., Pavri, B., Chovit, C., Solis, M., Olah, M., and Williams, O. Imaging spectroscopy and the airborne visible/infrared imaging spectrometer (AVIRIS). *Remote Sens. Environ.*, 65:227–248, 1998.
- [5] Cocks, T., Jenssen, R., Stewart, A., Wilson, I., and Shields, T. The hymap airborne hyperspectral sensor: the system, calibration and performance. In Remote Sensing Laboratories, U. o. Z., editor, *Proceedings of the First EARSeL Workshop on Imaging Spectroscopy*, pages 37–42, Zurich, Switzerland, 1998.
- [6] Richter, R. Geo-atmospheric processing of airborne imaging spectrometry data. part 2: atmospheric/topographic correction. *Int. J. Rem. Sen.*, 23:2631–2649, 2002.
- [7] Goetz, A. F. H., Kindel, B., Ferri, M., and Gutmann, E. Relative performance of HATCH and three other techniques for atmospheric correction of Hyperion and AVIRIS data. In *Summaries of the 11th Annual JPL Airborne Earth Science Workshop, AVIRIS Workshop*, Jet Propulsion Laboratory, Pasadena, CA, USA, 2003.
- [8] Boucher, Y., Poutier, L., Achard, V., Lenot, X., and Miesch, C. Validation and robustness of an atmospheric correction algorithm for hyperspectral images. In *Algorithms and Technologies for Multi-spectral, Hyperspectral and Ultraspectral Imagery VIII, SPIE AeroSense*, Orlando, FL, USA, 2002.
- [9] Ozone Processing Team. Total Ozone Mapping Spectrometer (TOMS) web page, 2004.
- [10] Aeronomy Laboratory, CMDL, CPC, and National Climatic Data Center. Stratospheric Ozone Monitoring and Research in NOAA, 2004.
- [11] Schläpfer, D., Borel, C. C., Keller, J., and Itten, K. I. Atmospheric pre-corrected differential absorption technique to retrieve columnar water vapor. *Remote Sens. Environ.*, 65:353–366, 1998.
- [12] Rodger, A. and Lynch, M. J. Determining atmospheric column water vapour in the 0.4–2.5 μm spectral region. In *Summaries of the 11th Annual JPL Airborne Earth Science Workshop, AVIRIS Workshop*, Jet Propulsion Laboratory, Pasadena, CA, USA, 2001.
- [13] Carrère, V. and Conel, J. E. Recovery of atmospheric water vapor total column abundance from imaging spectrometer analysis and application to Airborne Visible/Infrared Imaging Spectrometer (AVIRIS) data. *Remote Sens. Environ.*, 44:179–204, 1993.
- [14] Bojinski, S., Schläpfer, D., Schaepman, M., Keller, J., and Itten, K. Aerosol mapping over land with imaging spectroscopy using spectral autocorrelation. *Int. J. Rem. Sen.*, 20:5025–5047, 2004.
- [15] Isakov, V., Feind, R., Vasilyev, O., and Welch, R. Retrieval of aerosol spectral optical thickness from AVIRIS data. *Int. J. Rem. Sen.*, 17:2165–2184, 1996.
- [16] Green, R. Spectral calibration requirement for earth-looking imaging spectrometers in the solar-reflected spectrum. *Appl. Opt.*, 37:683–690, 1998.
- [17] Teillet, P. Image correction for radiometric effects in remote sensing. *Int. J. Rem. Sen.*, 7:1637–1651, 1986.
- [18] Smith, G. and Milton, E. The use of the empirical line method to calibrate remotely sensed data to reflectance. *Int. J. Rem. Sen.*, 20:2653–2662, 1999.
- [19] Cutter, M. Review of aspects associated with the chris calibration. In ESA/ESRIN, editor, *Proceedings of 2nd CHRIS/PROBA Workshop*, Frascati, Italy, April 2004.
- [20] Cutter, M. Personal communication. 2004.
- [21] Moreno, J. The SPECTRA Barrax Campaign (SPARC): Overview and first results from CHRIS data. In ESA/ESRIN, editor, *Proceedings of 2nd CHRIS/PROBA Workshop*, Frascati, Italy, April 2004.
- [22] World Meteorological Organization. A preliminary cloudless standard atmosphere for radiation computation. Technical Report WCP-112, World Climate Research Program, CAS, Radiation Commission of IAMAP, Boulder, CO, USA, 1986.
- [23] Vermote, E. F., Tanré, D., Deuzé, J. L., Herman, M., and Morcrette, J. J. Second simulation of the satellite signal in the solar spectrum, 6s: An overview. *IEEE Trans. Geosci. Remote Sens.*, 35:675–686, 1997.
- [24] Berk, A., Anderson, G. P., Bernstein, L. S., Acharya, P. K., Dothe, H., Matthew, M. W., Adler-Golden, S. M., Chetwynd, J. H., Richtsmeier, S. C., Pukall, B., Allred, C. L., Jeong, L. S., and Hoke, M. L. MODTRAN4 radiative transfer modeling for atmospheric correction. In *Proceedings of SPIE Optical Spectroscopic Techniques and Instrumentation for Atmospheric and Space Research III*, 1999.

- [25] Justice, C. O., Townshend, J. G. R., Holben, B. N., and Tucker, C. J. Analysis of the phenology of global vegetation using meteorological satellite data. *Int. J. Rem. Sen.*, 6:1271–1318, 1985.
- [26] Settle, J. On the dimensionality of multi-view hyperspectral measurements of vegetation. *Remote Sens. Environ.*, 90:235–242, 2004.
- [27] Thome, K., Palluconi, F., Takashima, T., and Masuda, K. Atmospheric correction of aster. *IEEE. Trans. Geosci. Remote Sens.*, 36:1199–1211, 1998.
- [28] Press, W. H., Flannery, B. P., Teukolosky, S. A., and Vetterling, W. T. *Numerical Recipes*. Cambridge University Press, 1986.
- [29] Vermote, E. F., Saleous, N. E., Justice, C. O., Kaufman, Y. J., Privette, J. L., Remer, L., Roger, J. C., and D.Tanré. Atmospheric correction of visible to middle infrared eos-modis data over land surface: Background, operational algorithm and validation. *J. Geophys. Res.*, 102:17131–17141, 1997.
- [30] Lee, T. Y. and Kaufman, Y. J. Non-lambertian effects in remote sensing of surface reflectance and vegetation index. *IEEE. Trans. Geosci. Remote Sens.*, 24:699–708, 1986.
- [31] Guanter, L., Martí, J. M., and Moreno, J. F. Atmospheric correction algorithm for multiangular satellite measurements in the solar spectrum. In *Conf. Remote Sensing, Proc. SPIE*, Barcelona, Spain, 2003.
- [32] Rast, M. SPECTRA - Surface Processes and Ecosystem Changes Through Response Analysis. ESA SP-1279(2), ESA-ESTEC, Noordwijk (The Netherlands), 2004.
- [33] Miller, J. R., Berger, M., Alonso, L., Cerovic, Z., Goulas, Y., Jacquemoud, S., Louis, J., Mohammed, G., Moya, I., Pedros, R., Moreno, J. F., Verhoef, W., and Zarco-Tejada, P. J. Progress on the development of an integrated canopy fluorescence model. In *Proceedings of IGARSS*, Toulouse (France), 2003.
- [34] Peña, R., Ruiz, A., and Domínguez, J. A. CEDEX proposal for CHRIS/PROBA activities in 2004 on validation of MERIS models. In *Proceedings of CHRIS/Proba Workshop*, ESA-ESRIN, Frascati (Italy), 2004.